Nonstoichiometry and Defect Chemistry of Ceria Solid Solutions

DANIEL SCHNEIDER, MARTIN GÖDICKEMEIER & LUDWIG J. GAUCKLER

ETH Zürich, Department of Materials, Institute of Nonmetallic Materials Swiss Federal Institute of Technology, CH-8092 Zürich, Switzerland

Abstract. Ceria solid solutions are potential electrolytes for solid oxide fuel cells (SOFC). At the anode side of SOFCs at low oxygen partial pressures ceria is partially reduced. The nonstoichiometry of CeO_{2-x} solid solutions with 20 mol% $SmO_{1.5}$, 20 mol% $GdO_{1.5}$ and 10 mol% CaO were investigated by isothermal coulometric titration in a zirconia cell in the temperature range from 700 to 900°C and in the oxygen partial pressure range from 10^{-12} to 10^{-25} atm.

The results of the 3 different compositions at 900°C are comparable to those for pure ceria. At lower temperatures, pure ceria is more stable against reduction than ceria solid solutions. The dependence of nonstoichiometry on oxygen partial pressure suggests a defect model with oxygen vacancies and their associates with reduced cerium cations and dopant cations. Low oxygen nonstoichiometries of x = 0.005 to 0.008 can be expected for ceria solid solutions at 700° under SOFC operating conditions.

I. Introduction

Conventional solid oxide fuel cells operate at temperatures above 900°C and use zirconia as an electrolyte. In order to reduce operating temperatures, ceria solid solutions were suggested as solid electrolytes [1–6] due to their higher ionic conductivity at temperatures below 800°C. However, under conditions prevailing at the anode side of SOFCs, they are reduced and become nonstoichiometric. The reduction of ceria introduces free electrons responsible for mixed ionic-electronic conductivity. Furthermore, reducing environment leads to an isothermal expansion of the material which can cause mechanical failure of ceria-based SOFC membranes and delamination of the electrodes.

The nonstoichiometry of pure, undoped ceria was investigated intensively [7–14]. Most of these studies were carried out using thermogravimetric methods [7–10] or solid state coulometric titration [13,14] to determine the extent of nonstoichiometry. For ceria solid solutions, on the other hand, only limited data on nonstoichiometry exist. Garnier et al. [15] and Park et al. [16] measured the reducibility of Ca substituted ceria at 800–1500°C by thermogravimetry and between 850 and 920°C by coulometric titration. Nonstoichiometry of Gd doped ceria at 1000°C, was investigated by Zachau-Christiansen et al. [17]. Bevan and Kordis [7] showed that pure ceria retains its cubic fluorite structure up to a nonstoichiometry of $x = 0.22$ at temperatures above 685°C. The partial enthalpy of oxygen of pure ceria $\Delta H(O_2)$, was calculated by Sorensen [9] as ~ -9.8 eV for small nonstoichiometries ($\log x = -2.6$). This is in good agreement with values around -10 eV at $\log x = -2.8$ found by Panlener et al. [8]. For 10 mol% calcia substituted ceria, on the other hand, a partial enthalpy of oxygen of -8.64 eV at $\log x = -2.59$ was found [16].

Different chemical defect models were suggested to describe the dependence of the nonstoichiometry on the oxygen partial pressure. Panlener et al. [8] and Panhans et al. [13] suggested a model considering only doubly ionized oxygen vacancies. Tuller and Nowick [18] used a model including interactions

between oxygen vacancies and quasi-free electrons introduced by the reduction.

The purpose of this study is to determine the nonstoichiometry of ceria solid solutions under SOFC operating conditions and to correlate the dependence of nonstoichiometry on oxygen partial pressure with a chemical defect model. Nonstoichiometry data of ceria solid solutions are obtained by solid state coulometric titration with a glass-sealed solid electrolyte coulometric titration cell. The results are interpreted by a chemical defect model also considering defect interactions.

II. Experimental

1. Powder Preparation

$Ce_{0.9}Ca_{0.1}O_{1.9-x}$ powder was prepared by wet-chemical coprecipitation from nitrate precursors. The materials were precipitated from an aqueous solution ($[Ce^{3+}] = 1\,M$, $[Ca^{2+}] = 0.11\,M$) of $Ce^{III}(NO_3)_3 \cdot 6H_2O$ (>99%, Fluka, Buchs, CH) and $Ca(NO_3)_2 \cdot 4H_2O$ (>99%, Merck, Darmstadt, FRG) using a 0.47 M solution of ammonium oxalate (>99.5 %, Fluka) at 45°C. This solution was washed three times with water at a pH of 8 and calcined at 750°C for 2 h. $Ce_{0.8}Sm_{0.2}O_{1.9-x}$ was prepared under the same conditions with a Sm–nitrate solution prepared from Sm_2O_3 (>99 %, Rhône-Poulenc, La Rochelle, F) dissolved in hydrochloric acid. $Ce_{0.8}Gd_{0.2}O_{1.9-x}$ powder was obtained from Rhône-Poulenc (Lot. No. 94007/99, La Rochelle). The composition was verified by microprobe analysis and by EDX. Compositions of the samples are given in Table 1. Pure ceria powder was obtained from a commercial source (>99.9%, Aldrich, Milwaukee, WI, USA).

Table 1. Composition and specific surface area of the powder samples

Sample	Composition (atom %)	Specific surface BET (m^2/g)	Grain size d_{50} (μm)
$Ce_{0.8}Sm_{0.2}O_{1.9}$	18.8 Sm 81.2 Ce	11.9	1.2
$Ce_{0.8}Gd_{0.2}O_{1.9}$	19.6 Ce 80.2 Ce 0.2 La	9.4	0.9
$Ce_{0.9}Ga_{0.1}O_{1.9}$	9.9 Ca 88.9 Ce 1.2 Zr	10.5	2.5

2. Solid-state coulometric titration

2.1. Experimental setup.
The experimental setup with the coulometric titration cell is shown in Fig. 1. The cell consists of an alumina tube, 14.5 mm in diameter and 20.8 mm high, which is closed at one end. The top of the cell is an 8 mole% yttria stabilized zirconia (YSZ) solid electrolyte disk with a thickness of 1 mm. On both sides of the electrolyte, platinum paste (Heraeus C 3605 S) was applied, as electrodes. The inner electrode was connected to the measurement circuit through the seal.

The measurement setup is shown in Fig. 1. It consists of a programmable power supply (GPM 6030, Good Will Instrument CO., Taiwan) and a scanning digital multimeter (Keithley, DMM 2001) equipped with a 10 channel scanning card for the detection of electrical current and EMF. The measurement of the EMF and the integration of current over time was computerassisted. The sample was placed in an electrically heated furnace and the temperature was controlled by a thermocouple placed on top of the solid electrolyte. The solid electrolyte with the platinum electrodes served alternatively as an oxygen pump as well as an EMF sensor.

2.2. Measurement.
Approximately 4 g of sample powder was weighted into the cell. In order to seal the cell an organic slurry containing a glass (Cerdec 90016, Degussa, Frankfurt, FRG) with good wettability for zirconia and alumina was applied between the lid and the crucible. The slurry consisted of a
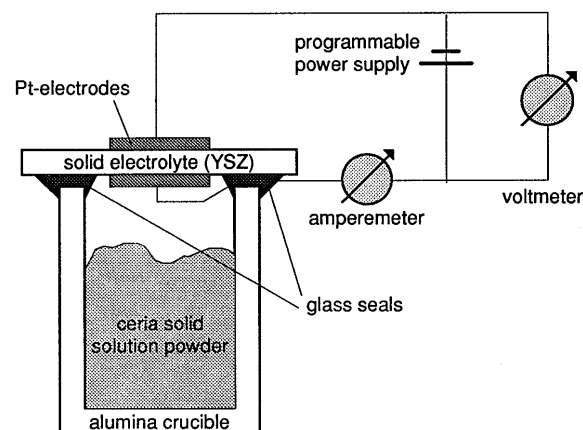

Fig. 1. Solid electrolyte coulometric titration cell for the nonstoichiometry measurements.

mixture of ethanol (23wt.%) PVB (2wt.% Mowital B20H, Hoechst, Frankfurt, FRG) and glass powder (75wt.%).

The cell was heated to 920°C and then slowly cooled down to 900°C. In a first coulometric titration run oxygen was removed from the cell. The gas-tightness of the cell was verified by following the EMF vs. time. When a steady state was reached, i.e. the EMF decreased by less than 0.3 mV/min the cell was judged to be sufficiently gas-tight. If the EMF change was higher, the cell was again cooled down to room-temperature and another layer of glass paste was applied. This procedure was repeated until a gas-tight cell was obtained. With this easy cell assembly only about 20% of the cells were gas-tight for the first time and the sealing procedure had to be performed up to 5 times to obtain gas-tight cells.

The cell was cooled down to the measurement temperature at 0.5°C/min. Higher cooling rates led to cracking of the glass seal, especially at temperatures below 800°C. After reaching the measuring temperature of 700, 800 or 900°C, the cells were held at this temperature for at least 30 min to enable temperature stabilization.

The cells were short circuited until the EMF was zero, i.e. the oxygen partial pressure at the inner electrode corresponded to that at the outer electrode. The composition of the samples was assumed to be stoichiometric under these conditions.

For the nonstoichiometry measurements, oxygen was removed from the cell using a current of 5 to 15 mA. The amount of oxygen was determined by integrating the electrical current over time. After a preset time the current was switched off and the stabilization of the EMF over time was observed until equilibrium was reached. A change of EMF of less than 0.2–0.3 mV per minute was taken as equilibrium criterion. Normally the equilibrium criterion was fulfilled after 60–200 min at 700°C and 40–80 min at 900°C.

The calibration of the cell (leakage rate) has been made as follows: After the last titration step of every measurement the EMF was measured for an extended period of 8 h.

Measurements were carried out with $Ce_{0.8}Sm_{0.2}O_{1.9}$, $Ce_{0.8}Gd_{0.2}O_{1.9}$ and $Ce_{0.9}Ca_{0.1}O_{1.9}$ at 700, 800 and 900°C. A typical example of the time needed for equilibration is given in Fig. 2 for a $Ce_{0.8}Gd_{0.2}O_{1.9-x}$ sample at 700°C. A measurement run with the titration period (a) and the equilibration

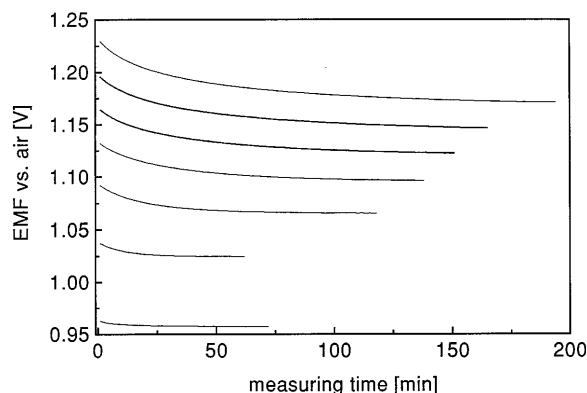*Fig. 2.* EMF measured over the YSZ-electrolyte after the titration current was switched off ($t = 0$) for different titration runs ($Ce_{0.8}Gd_{0.2}O_{1.9-x}$ at 700°C).

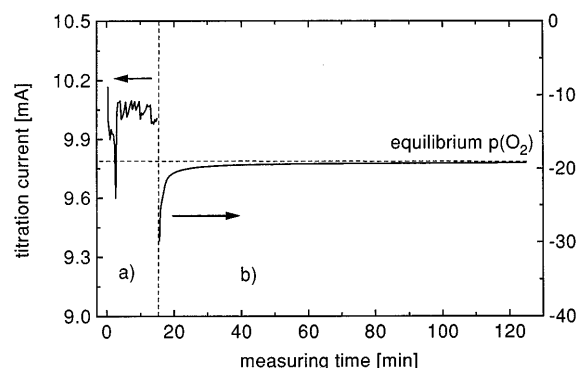*Fig. 3.* Coulometric titration run with (a): titration period and (b): equilibration period.

period (b) is given in Fig. 3 for $Ce_{0.9}Ca_{0.1}O_{1.9-x}$ at 700°C.

III. Results and Discussion

The dependence of the nonstoichiometry on the oxygen partial pressure ($p(O_2)$) was calculated. The nonstoichiometry x vs. $p(O_2)$ is shown in Figs. 4a–c for $Ce_{0.8}Sm_{0.2}O_{1.9-x}$, $Ce_{0.8}Gd_{0.2}O_{1.9-x}$ and $Ce_{0.9}Ca_{0.1}O_{1.9-x}$ together with literature data for pure CeO_{2-x} at 900, 800, and 700°C. The plotted data are maximum values because the nonstoichiometry x was calculated on the condition that no leakage of oxygen occurs. The error bars in Figs. 4a–c were estimated from the calibration measurements described in the preceding section.

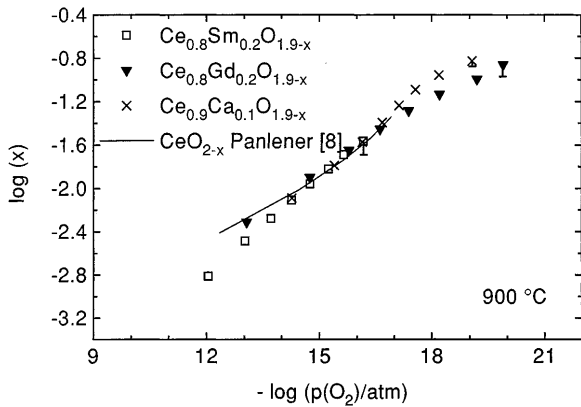Among the different ceria solid solutions, only small differences in nonstoichiometry are found. The

Fig. 4a. Oxygen nonstoichiometry vs. $\log(p(O_2))$ at 900°C for ceria solid solutions with Ca^{2+}, Sm^{3+} and Gd^{3+} and pure ceria (Ref. 8).
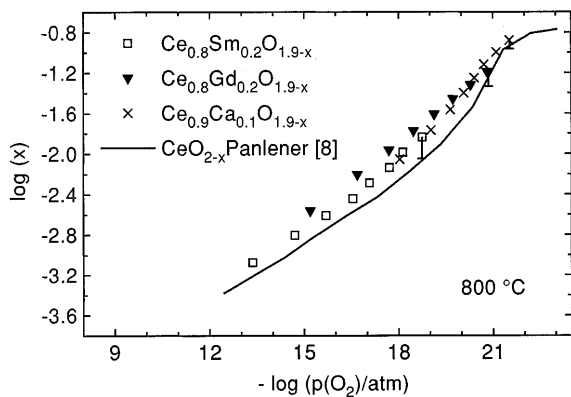

Fig. 4b. Oxygen nonstoichiometry vs. $\log(p(O_2))$ at 800°C for ceria solid solutions with Ca^{2+}, Sm^{3+} and Gd^{3+} and pure ceria (Ref. 8).
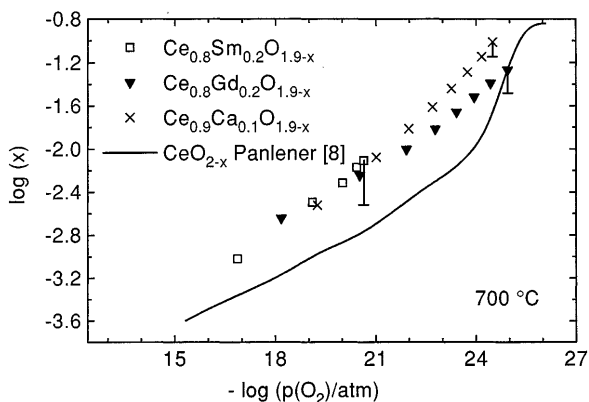

Fig. 4c. Oxygen nonstoichiometry vs. $\log(p(O_2))$ at 700°C for ceria solid solutions with Ca^{2+}, Sm^{3+} and Gd^{3+} and pure ceria (Ref. 8).
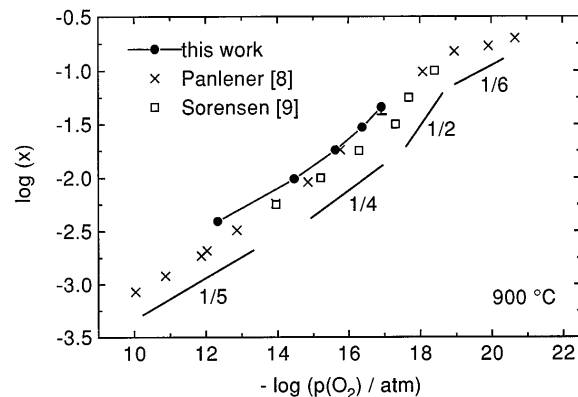

Fig. 5. Dependence of nonstoichiometry of undoped ceria on oxygen partial pressure, as compared to literature data from thermogravimetric measurements at 900°C.

difference between the ceria solid solutions and pure ceria, however, increases with decreasing temperature. At 900°C, pure ceria and ceria solid solutions show the same stability against reduction. At lower temperatures pure ceria is more stable than ceria solid solutions, which means that the partial enthalpy of oxygen is higher for pure ceria than for its solid solutions. This is in accordance with findings of Sorensen (9) and Park et al. (8), who found a partial enthalpy of oxygen of -9.8 to $-10\,eV$ at $\log(x) = 2.6$ for pure ceria, and Garnier (15) or Park (16), who found a partial enthalpy of oxygen of $-8.64\,eV$ at $\log(x) = 2.6$ for $10\,mol\%$ CaO doped ceria. Assuming a simple defect model as presented in section 4 of this chapter (see Eqs. 7–10) partial enthalpies of oxygen $\Delta H(O_2)$ of $-7.45\,eV$, $-7.26\,eV$ and $-7.24\,eV$ are found for $Ce_{0.8}Gd_{0.2}O_{1.9-x}$, $Ce_{0.9}Ca_{0.1}O_{1.9-x}$ and $Ce_{0.8}Sm_{0.2}O_{1.9-x}$ at $\log x = -2.6$.

For comparison, coulometric titration measurements with pure CeO_{2-x} were carried out at 900°C, and were compared to literature data obtained by thermo-gravimetric measurements. Figure 5 shows these datas in the form of nonstoichiometry versus oxygen partial pressure. The data for pure ceria obtained in this work is in good agreement with other literature data [8,9]. The slope of the curves in Figure 5 was found to increase from $\sim1/5$ at higher oxygen partial pressures to $\sim1/2$ at $p(O_2)$ around 10^{-16} atm. At oxygen partial pressures lower than 10^{-18} atm the slope decreases again.

In Figs. 6 and 7 the reciprocal of the slope of $\log(x)$ vs. $-\log(p(O_2))$ is plotted at 900°C for experimental data as well as calculated data. It is given as $m(x) = d\log p(O_2)/d\log(x)$ (Eq. 11). For pure ceria
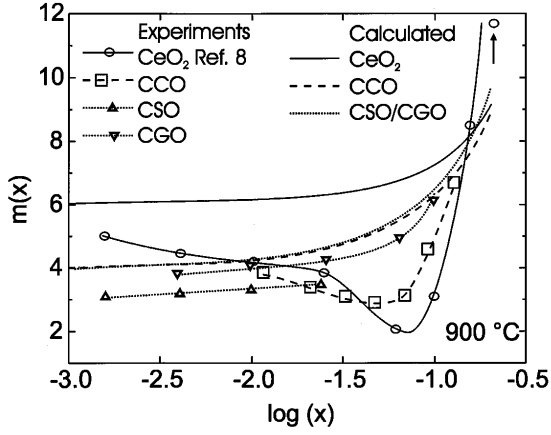
Fig. 6. Reciprocal slope $m(x) = d \log p(O_2)/d \log(x)$ for pure ceria (Ref. 8) and ceria solid solutions with Ca^{2+}, Sm^{3+} and Gd^{3+} (CCO, CSO, CGO) at 900°C as well as data calculated with the simple defect model (Eqs. 12 and 13).

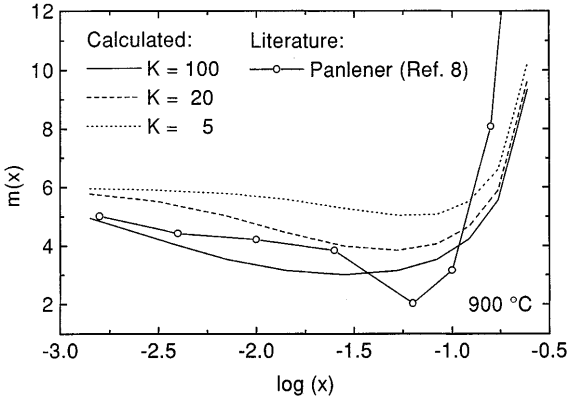*Fig. 7a.* Reciprocal slope $m(x) = d \log p(O_2)/d \log(x)$ for pure ceria (Ref. 8) at 900°C as well as calculated data based on a defect model with associated defects (Eq. 22).

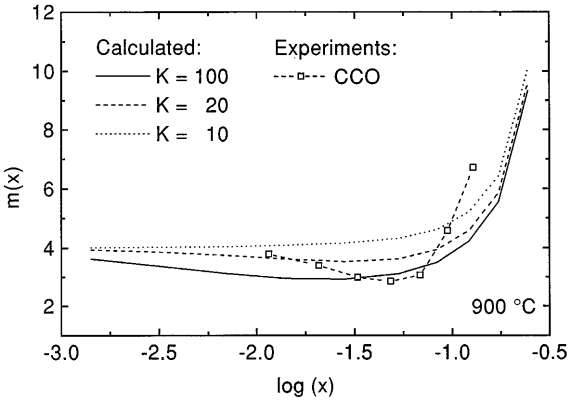*Fig. 7b.* Reciprocal slope $m(x) = d \log p(O_2)/d \log(x)$ for ceria-calcia solid solutions (CCO) at 900°C as well as calculated data based on a defect model with associated defects (Eq. 21).

(Ref. [8]) and $Ce_{0.9}Ca_{0.1}O_{1.9-x}$ a minimum of $m(x)$ is observed at $\log(x) = -1.2$ and $\log(x) + -1.4$, respectively. For $Ce_{0.8}Gd_{0.2}O_{1.9-x}$ and $Ce_{0.8}Sm_{0.2}O_{1.9-x}$ $m(x)$ increases from 4 for small deviations from stoichiometry to values comparable to pure ceria and $Ce_{0.9}Ca_{0.1}O_{1.9-x}$. In the next section, chemical defect models are presented, to explain this behavior.
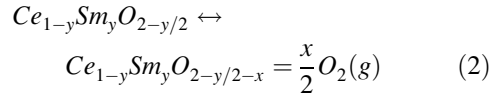
IV. Defect Models

In this section defect models are derived for pure ceria and ceria solid solutions with divalent or trivalent dopants. First a simple defect model is presented which, however, cannot explain the different slopes of the nonstoichiometry curves presented in Fig. 6. Therefore, in a second step the simple model is extended by allowing defect interactions.

1. Simple Defect Model

The overall reduction reaction for ceria solid solutions with divalent dopants (Ca^{2+}) is

$$Ce_{1-y}Ca_yO_2 \leftrightarrow Ce_{1-y}Ca_yO_{2-y-x} + \frac{x}{2}O_2(g) \quad (1)$$
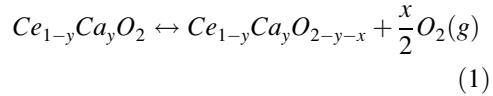
For trivalent dopants (e.g. Sm^{3+}) this reaction is

$$Ce_{1-y}Sm_yO_{2-y/2} \leftrightarrow$$
$$Ce_{1-y}Sm_yO_{2-y/2-x} = \frac{x}{2}O_2(g) \quad (2)$$

The site fractions of the different species can be expressed as follows:

$$[Ce_{Ce}^x] = 1 - y - 2x \quad (3)$$

$$[Ce_{Ce}'] = 2x \quad (4)$$

$$[O_O^x] = \tfrac{1}{2}(2 - x - y) \text{ and}$$
$$[V_{\ddot{O}}] = \tfrac{1}{2}(x + y) \text{ for divalent dopants} \quad (5a)$$

$$[O_O^x] = \tfrac{1}{2}(2 - x - y/2) \text{ and}$$
$$[V_{\ddot{O}}] = \tfrac{1}{2}(x + y/2) \text{ for trivalent dopants} \quad (5b)$$

The reduction reaction in Kröger-Vink notation is

$$2Ce_{Ce}^x + O_O^x \xrightarrow{K_1} 2Ce_{Ce}' + V_{\ddot{O}} + \tfrac{1}{2}O_2(g) \quad (6)$$
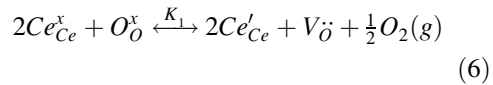
The mass action constant associated with the above reaction for divalent dopants is given as

$$K_1(Ca) = \frac{4x^2 \cdot (x+y) \cdot p(O_2)^{1/2}}{(1-y-2x)^2 \cdot (2-y-x)} \qquad (7)$$

For trivalent dopants the mass action constant is given as

$$K_1(Sm) = \frac{4x^2 \cdot (x+y/2) \cdot p(O_2)^{1/2}}{(1-y-2x) \cdot (2-y/2-x)} \qquad (8)$$

The corresponding relative Gibbs free energy of oxygen $\Delta G(O_2)$ can be given as

$$\Delta G(O_2) = 2kT \ln(K_1) \qquad (9)$$

By a linear fitting of a plot of $\ln(K_1)$ vs. $1/T$ one can obtain the corresponding relative enthalpy and entropy of oxygen according to

$$\Delta G(O_2) = \Delta H(O_2) - T\Delta S(O_2) \qquad (10)$$

Values for the relative enthalpy of oxygen have already been given in section 3, but since only three temperatures were measured they are not very accurate.

Simplifying the relation between $p(O_2)$ and x (Eq. 7,8), under the assumption that doubly ionized vacancies are dominating, we get

$$x \propto p(O_2)^{-1/m(x)} \qquad (11)$$

where $m(x)$ is the reciprocal slope in the plot $\log(x)$ vs. $-\log(p(O_2))$ for divalent dopants

$$\begin{aligned} m(x) &= -\frac{d\log(p(O_2))}{d\log(x)} \\ &= 4 + \frac{2x}{x+y} + \frac{8x}{1-y-2x} \\ &\quad + \frac{2x}{2-y-x} \end{aligned} \qquad (12)$$
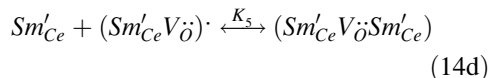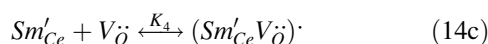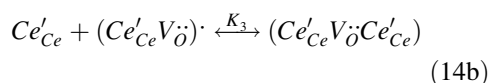
and for trivalent dopants

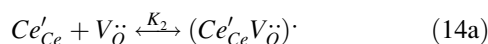$$\begin{aligned} m(x) &= -\frac{d\log(p(O_2))}{d\log(x)} \\ &= 4 + \frac{2x}{x+y/2} + \frac{8x}{1-y-2x} \\ &\quad + \frac{2x}{2-y/2-x} \end{aligned} \qquad (13)$$

From Eqs. (12) and (13) it follows, that for small deviations from stoichiometry the slope $\log(x)$ vs. $\log(p(O_2))$ is $1/m(x) = 1/6$ for pure CeO_{2-x} and $1/4$ for ceria solid solutions with divalent and trivalent dopants ($y \gg x$). In Fig. 6 the calculated reciprocal

slopes $m(x)$ for pure and doped ceria are shown. Using the simple defect model an increasing reciprocal slope $m(x)$ is expected for increasing nonstoichiometry. This is in contradiction to the experimental findings for pure ceria and calcia doped ceria, and obviously the applied simple defect model has to be modified including defect interactions such as vacancy clustering and defect association.

2. Associated Defects

Defects of opposite charge may form defect complexes in the ceria lattice due to their electrostatic interactions [19,20]. Oxygen vacancies can form associates with one or two trivalent cations. These cations can either be reduced host cations or trivalent dopants such as Sm^{3+} or Gd^{3+} (Eqs. 14a–d).

$$Ce'_{Ce} + V_{\ddot{O}} \xleftrightarrow{K_2} (Ce'_{Ce}V_{\ddot{O}})^{\cdot} \qquad (14a)$$

$$Ce'_{Ce} + (Ce'_{Ce}V_{\ddot{O}})^{\cdot} \xleftrightarrow{K_3} (Ce'_{Ce}V_{\ddot{O}}Ce'_{Ce}) \qquad (14b)$$

$$Sm'_{Ce} + V_{\ddot{O}} \xleftrightarrow{K_4} (Sm'_{Ce}V_{\ddot{O}})^{\cdot} \qquad (14c)$$

$$Sm'_{Ce} + (Sm'_{Ce}V_{\ddot{O}})^{\cdot} \xleftrightarrow{K_5} (Sm'_{Ce}V_{\ddot{O}}Sm'_{Ce}) \qquad (14d)$$

With divalent dopants, such as Ca^{2+} neutral defect complexes are formed according to Eq. 14e.

$$Ca''_{Ce} = V_{\ddot{O}} \xleftrightarrow{K_6} (Ca''_{Ce}V_{\ddot{O}}) \qquad (14e)$$
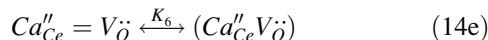
K_2 to K_6 are the appropriate equilibrium constants for Eqs. 14a–e.

The electroneutrality condition (Eq. 15), the dopant concentration (Eq. 16) and the oxygen nonstoichiometry (Eq. 17) are expressed by the following equations for the example of divalent doping:

$$2 \cdot [Ca''_{Ce}] + [Ce'_{Ce}] = [(Ce'_{Ce}V_{\ddot{O}})^{\cdot}] + 2 \cdot [V_{\ddot{O}}] \qquad (15)$$

$$[Ca''_{Ce}] + [(Ca''_{Ce}V_{\ddot{O}})] = y \qquad (16)$$

$$\begin{aligned} [Ce'_{Ce}] + [(Ce'_{Ce}V_{\ddot{O}})^{\cdot} + 2 \cdot [(Ce'_{Ce}V_{\ddot{O}}Ce'_{Ce})] \\ = 2x \end{aligned} \qquad (17)$$

From Eqs. 14–17 a system of 3 equations is obtained to express the oxygen nonstoichiometry including defect interactions:

$$2 \cdot [Ca''_{Ce}] + [Ce'_{Ce}] = K_2 \cdot [Ce'_{Ce}] \cdot [V_{\ddot{O}}] + 2 \cdot [V_{\ddot{O}}] \tag{18}$$

$$[Ca''_{Ce}] + K_6 \cdot [Ca''_{Ce}] \cdot [V_{\ddot{O}}] = y \tag{19}$$

$$[Ce'_{Ce}] + K_2 \cdot [Ce'_{Ce}] \cdot [V_{\ddot{O}}] + 2K_2K_3 \cdot Ce'_{Ce}]^2 \cdot [V_{\ddot{O}}] = 2x \tag{20}$$

Analogue equations can be formulated for trivalent dopants.

For given parameters $K_1 - K_6$ (Eqs. 6, 14a–e), y, and x this system can be solved and with Eq. 6 and Eqs. 14–17 the dependence of $\log(p(O_2))$ on $\log(x)$ is expressed as follows:

$$\log(p(O_2)) - 2\log K_1 = \\ -2\log\left(\frac{[Ce'_{Ce}]^2 \cdot [V_{\ddot{O}}]}{(1-y-2x)^2 \cdot (2-y-x)}\right) \tag{21}$$

Equivalent equations for pure ceria ($y = 0$) as well as for ceria solid solutions with trivalent oxides can be calculated. For these solid solutions one obtains:

$$\log(p(O_2)) - 2\log K_1 = \\ -2\log\left(\frac{[Ce'_{Ce}]^2 \cdot [V_{\ddot{O}}]}{(1-y-2x)^2 \cdot (2-y/2-x)}\right) \tag{22}$$

Results of the calculations for pure ceria and ceria solid solutions with divalent oxides with different K_1 to K_6 are shown in Fig. 7a and 7b. Several calculations showed that the parameters K_4, K_5 and K_6 have only small influence on the shape of the curve. They were therefore assumed equal to K_2 for trivalent and to K_2^2 for divalent dopants. The oxygen partial pressure was normalized by K_1. It is shown in this figure, that an association of Ce^{3+} with oxygen vacancies leads to a decrease in oxygen vacancy activity model in an intermediate nonstoichiometry region ($-2 < \log(x) < -1.2$) and therefore to a steeper increase of the nonstoichiometry with decreasing $p(O_2)$ than for the simple defect. At higher nonstoichiometries ($\log(x) > -1.2$) the slopes of $\log(x)$ vs. log ($p(O_2)$) flatten again. Higher assumed values for defect association constants would lead to steeper slopes of the non-stoichiometry curves.

At very low nonstoichiometries, the defect inter-actions are small and therefore the slopes of the nonstoichiometry curves approach the one expected from Eq. 13, that is $-1/4$ for doped ceria and $-1/6$ for pure ceria. As shown in Fig. 4 the defect interaction, indicated by a steeper slope, increases with decreasing temperature and increases from $Ce_{0.8}Gd_{0.2}O_{1.9-x}$ and $Ce_{0.8}Sm_{0.2}O_{1.9-x}$ to $Ce_{0.9}Ca_{0.1}O_{1.9-x}$ and pure CeO_{2-x}. Therefore, $Ce_{0.9}Ca_{0.1}O_{1.9-x}$ exhibits the highest oxygen nonstoichiometry at low oxygen partial pressures for all three solid solutions examined in this study.

V.   Conclusions

Ceria solid solutions show a slightly lower relative enthalpy of oxygen compared to pure ceria. This leads to a higher nonstoichiometry at 700 and 800°C, while nonstoichiometry was found to be equal to pure ceria at 900°C. To obtain quantitative data for the relative enthalpy and entropy of oxygen, more measurements in a wider temperature range would be necessary.

Data of nonstoichiometry obtained in this work by the use of coulometric titration agree very well with literature data obtained by thermogravimetry. The dependence of the log of nonstoichiometry of ceria solid solutions on log of the oxygen partial pressure deviates slightly from $-1/4$, a value which would be expected for the simple defect model without defect interactions. The deviation is more pronounced for ceria-calcia solid solutions than for ceria-gadolinia and ceria-samaria solid solutions.

The steeper slope $1/m(x)$ at nonstoichiometries between $0.01 < x < 0.06$ at temperatures between 700–900°C can be explained by association of oxygen vacancies with Ce^{3+} cations. This was confirmed by calculations. The great size misfit of Ce^{3+} cations and their higher mobility lead to a high tendency to form defect clusters whereas the dopant cations provide oxygen vacancies [21]. However, similar results might be obtained assuming clusters of oxygen vacancies which might be formed at higher oxygen vacancy concentrations [22]. For ceria-calcia solid solutions a stronger defect association was found than for ceria-gadolinia solid solutions.

The nonstoichiometry of ceria solid solutions under SOFC operating conditions (10^{-20} atm, 700°C) is about 0.005 corresponding, to a linear isothermal expansion of the lattice of 0.05% [23] which seems tolerable for SOFC application. It even

may be speculated, that a slight reduction causes a useful electronic conductivity on the surface of the anode side of the electrolyte.

Acknowledgments

References

1. D. Singman, *J. Electrochem. Soc.*, **113**, 502 (1966).
2. R.N. Blumenthal, F.S. Brugner and J.E. Garnier, *J. Electrochem. Soc.*, **120**, 1230 (1973).
3. H.L. Tuller and A.S. Nowick, *J. Electrochem. Soc.*, **122**, 255 (1975).
4. T. Kudo and Y. Obayashi, *J. Electrochem. Soc.*, **123**, 415 (1976).
5. R.T. Dirstine, R.N. Blumenthal and T.F. Kuech, *J. Electrochem. Soc.*, **126**, 264 (1979).
6. M.D. Hurley and D.K. Hohnke, *J. Phys. Chem. Solids*, **41**, 1349 (1980).
7. D.J.M. Bevan and J. Kordis, *J. Electrochem. Soc.*, **26**, 1509 (1964).
8. R.J. Panlener, R.N. Blumenthal and J.E. Garnier, *J. Phys. Chem. Solids*, **36**, 1213 (1975).
9. O.T. Sorensen, *J. Solid State Chem.*, **18**, 217 (1976).
10. I.K. Naik and T.Y. Tien, *J. Phys. Chem. Solids*, **39**, 311 (1978).
11. M. Ricken, J. Nölting and I. Riess, *J. Solid State Chem.*, **54**, 89 (1984).
12. J.W. Dawicke and R.N. Blumenthal, *J. Electrochem. Soc.*, **133**, 904 (1988).
13. M.A. Panhans and R.N. Blumenthal, *Solid State Ionics*, **60**, 279 (1993).
14. H. Janczikowski, *PhD thesis*, Georg-August-Universitðt, Göttingen, Germany, 1985.
15. J.E. Garnier, R.N. Blumenthal, R.J. Panlener and K.R. Sharma, *J. Phys. Chem. Solids*, **37**, 369 (1976).
16. J.-H. Park, R.N. Blumenthal and M. A. Panhans, *J. Electrochem. Soc.*, **135**, 855 (1988).
17. B. Zachau-Christiansen, T. Jacobsen, K. West and S. Skaarup, pp. 104-11 in Proceedings of the Third International Symposium on Solid Oxide Fuel Cells, Honolulu, Hawaii, May, 1993. Edited by S. C. Singhal and H. Iwahara. The Electrochemical Society, Pennington, NJ, 1993.
18. H.L. Tuller and A. S. Nowick, *J. Electrochem. Soc.*, **126**, 209 (1979).
19. W.D. Kingery, H.K. Bowen and D.R. Uhlmann, *Introduction to Ceramics* John Wiley & Sons, New York, 2nd, 1976, p. 148.
20. S. Ling, *Physical Review B*, **49**, 864 (1994).
21. P. Li, I-W. Chen, J. E. Penner-Hahn and T.-Y. Tien, *J. Am. Ceram. Soc.*, **74**, 958 (1991).
22. C.R.A. Catlow, p. 66 in Materials Science Series, *Nonstoichiometric Oxides*. Edited by O. T. Sorensen. Academic Press, New York, 1981.
23. H.-W. Chiang, R.N. Blumenthal and R.A. Fournelle, *Solid State Ionics*, **66**, 85 (1993)